Universiteit Leiden

The Netherlands

Surface temperature and the dynamics of H2 on Cu(111)
Smits, B.

Citation

Smits, B. (2023, July 4). *Surface temperature and the dynamics of H2 on Cu(111)*. Retrieved from https://hdl.handle.net/1887/3628423

Chapter 5

The quantum dynamics of H_2 on Cu(111) at a surface temperature of 925 K: Comparing theory to experiments

Abstract

We present results of our recently expanded static corrugation model (SCM) approach that included the relevant surface temperature effects, applied to the dissociative chemisorption reaction of H_2 on a Cu(111) surface. The reaction and rovibrationally elastic scattering probabilities that we obtain at a quantum dynamical (QD) level, as an average of many statically distorted surface configurations, show great agreement with those of a dynamic surface model. This greatly reinforces the validity of the sudden approximation inherent to the SCM. We further investigate several simple methods of binning the final rovibrational state of quasi-classical dynamics simulations to find those best suited to reproduce the QD results for our system. Finally, we show that the SCM obtained results reproduce experimental dissociation curves very well when the uncertainty in experimental saturation values is taken into account. Some indication of a slow channel, so far only observed in experiment, can also

be found at low incidence energies, although more rigorous QD simulations are required to reduce the noise inherent to our propagation methods.

5.1   Introduction

Heterogeneous catalysis is one of the backbones of modern life, being vital in processes such as steam reforming, for H_2 production, and the Haber-Bosch process, for the production of fertilisers[1, 2]. Here the accurate modelling of gas-surface dissociation reactions is an important topic, as it is often the rate-limiting elementary step in these reactions[3]. Past works often relied on simple static and ideal surface models to describe the elementary reactions, neglecting the potentially important effects of energy exchange with the surface or thermal distortion of the surface. As industrial heterogeneous catalysis processes generally take place well above 0 K, further gains in the description of these simple dissociation reactions can be attained by finding accurate models for describing surface temperature effects[4].

For this chapter, our system of choice is once again the dissociative chemisorption of H_2 on a (thermally excited) Cu(111) surface. This system is one of the model systems in the field of surface science, with an array of experimental[5–12] and theoretical[13–26] data available. In particular, Kaufmann *et al.* recently presented experimental results that allowed them to fully characterise a slow reaction channel for the system, which shows strong temperature and vibrational dependencies, but has not yet been observed in any theoretical works[11]. Similarly, Chadwick *et al.* recently published sharply defined state-to-state diffraction probabilities at a surface temperature of 130 K, using their molecular interferometry setup[12, 27].

For this chapter we have chosen to make use of the SCM approach to describe the effect of surface temperature on the H_2/Cu(111) system, as it has been shown to be accurate at both a QC and a QD level for not only dissociation but also rovibrationally elastic scattering probabilities[15, 18]. Our ideal lattice 6D potential energy surface (PES) of choice was fitted by Nattino *et al.* using the corrugation reducing procedure (CRP)[28], with a dataset obtained using density functional theory (DFT) and the SRP48 functional[29]. SRP48 has already shown to reproduce experimental results to within chemical accuracy with the Born-Oppenheimer static surface (BOSS) approach, where the electron and nuclear dynamics are assumed to be fully separable and the surface atoms are kept static at their ideal lattice positions[30]. The SCM then expands on this potential through the addition of a coupling potential, also fit to SRP48 DFT data, which describes the effect of distorting the surface due to thermal effects[20]. Surface configurations are obtained using an embedded

atom method (EAM) potential, which has been shown to accurately reproduce various observables for the copper surface[31]. Electronic friction due to electron-hole pair excitations has been shown to not be relevant for this system, and is thus not included in this model[32].

One of the main assumptions of this EAM-SCM approach is that the Cu(111) surface dynamics can be treated at a sudden approximation level, where the surface atoms are not allowed to move. However, the EAM potential can also be used to describe surface motion during dynamics, as the EAM-SCM could be further expanded to the dynamic corrugation model (DCM). Previous work comparing the results obtained with the EAM-SCM and EAM-DCM [for D_2 on Cu(111)] validated the sudden approximation that lies at the base of the SCM, and proved the limited effect energy exchange with the surface has on this system[15]. Recent work has also shown the SCM to hold well when applied to 6D QD simulations with a statically distorted surface, when treating the incoming H_2 at its rovibrational ground state, although there were some clear differences found between the QC and QD results for the rovibrationally elastic scattering probabilities[18].

While we will only treat the H_2/Cu(111) system, the EAM-SCM approach is expected to be general enough to be used for the reaction of other diatomic molecules reacting on a transition metal surface. In particular, the model is expected to perform well when energy exchange with the surface plays only a minimal effect, either due to a large mass mismatch between the surface atoms and the reactant, and/or due to short interaction times with the surface. It also relies on the availability of (a dataset of) accurate DFT results that can be used to both construct the BOSS PES, and fit the required SCM potential to statically include the surface temperature effects. For Cu, in particular, previous work has already shown that the SRP48 functional is transferable to other Cu facets, and thus would be an excellent target for future work[33, 34]. The thermally distorted surface configurations needed for the SCM can be obtained from a variety of sources, such as simple force-fields methods, or constructed using, for example, the Debye-Waller factor[20]. For those systems where energy exchange with the surface is important the DCM would be required, which would then also require a potential to accurate describe the motion of the surface atoms. This has, however, only been tested for the H_2 and D_2 on Cu systems so far, and is only computationally viable at a (quasi-)classical level due to the large number of surface DoF involved[15]. Similarly, we expect electronic frictions models to be able to expand the EAM-SCM, although this is currently also only possible at a classical dynamics level[35–37].

In this chapter I present dissociation and elastic scattering probabilities of H_2 on a (thermally distorted) Cu(111) surface slab, obtained using the BOSS

approach and EAM-SCM approach at a modeled surface temperature of 925 K, both using QD and QCD simulations. To complement the results of the previously published rovibrational ground state (of H_2), we now also investigate several initial rovibrationally excited states. Static surface EAM-SCM results are compared to EAM-DCM results where the surface is allowed to move, to further verify the quality of the sudden approximation for this system [which had so far only been shown for the D_2/Cu(111) system]. Several rovibrational binning methods are applied to the final classical state of the QCD results, and compared to the exact quantised 6D simulations to verify the quality of these binning methods when applied to the H_2/Cu(111) system. Finally, the QD- and QCD-EAM-SCM dissociation probability curves are compared to those obtained from the direct inversion of desorption experiments at the same surface temperature, both at higher incidence energies and at very low reaction probabilities near the curve onset.

5.2 Method

In this chapter, we will continue on the results of Chapter 4, now including QD and QCD results for (ro)vibrationally excited initial states. For the QD and QCD results we once again make use of the TDWP approach and the quasi-classical dynamics approach as discussed in respectively sections 2.1.3 and 2.2.1 of Chapter 2. We will also compare to dissociation and scattering probabilities obtained using the moving surface EAM-DCM approach.

The same SRP48 CRP PES as used in the previous chapters is again applied, as well as the effective three-body SCM coupling potential as described by Spiering *et al.*[25]. Similarly, the database of thermally distorted surface slabs, constructed as described in Chapter 3, is used to obtain the EAM-SCM (and -DCM) surface configurations, with the same 16 bohrs ($\sim$ 8.47 Å) cutoff distance.

5.2.1 Quantum dyanmics

To obtain a single representative dissociation or scattering curve for H_2 reacting with thermally distorted Cu(111) at a QD level, we average the probabilities obtained for a total of 104 unique thermally distorted surface slabs. By averaging over the results obtained from these thermally distorted surface slabs, the quantum dynamics of the surface atom degrees of freedom is effectively done on a sudden approximation level using Monte-Carlo sampling. Thus we essentially perform QD implicitly even for the surface degrees of freedom, but with the approximation that energy exchange between H_2 and the surface is not possible.

Furthermore, there is also no energy exchange possible between the vibrations within the solid during the individual QD TDWP runs, making sure that any classical redistribution or leaking of zero point energy is not possible at all. This is where we think the SCM shines compared to other models, employing thermostats and/or other RPMD assumptions (i.e. using Boltzmann statistics and harmonic potentials) especially relevant for $T_s < 300$ K for Cu.

For each individual surface configuration, the QD reaction or elastic scattering curve is obtained via three different WPs, one with an energy range 0.10 to 0.30 eV, another 0.25–0.70 eV, and a third 0.65–1.00 eV, as already used in the previous chapter on the rovibrational ground state. For the initial rotationally excited states only those states with $mJ \geq 0$ were considered, with the results for $mJ \neq 0$ counted twice in the total average per rotational state, to account for the $mJ < 0$ states. Details regarding the computational parameters for each of these wave packets can be found in the appendix (6.A) of Chapter 6.

5.2.2 Final state binning

There will also be a bigger focus on different methods of binning the final rovibrational state of the QCD calculations, as also outlined in 2.2.4 of Chapter 2. Here first the modulus of the classical angular momentum ($|L_f|$) is calculated

$$|L_f|^2 = p_\theta{}^2 + \frac{p_\phi{}^2}{\sin^2 \theta} \tag{5.1}$$

where p_θ and p_ϕ describe the conjugate momenta along the two molecular angles. This angular momentum is then used to determine a classical "rotational state"

$$J_f = \frac{\sqrt{1 + 4|L_f|^2} - 1}{2} \tag{5.2}$$

which is found by equating $|L_f|^2$ to $J(J+1)$.

Next this classical state is binned using one of three methods. Using the standard binning method, which is how we have performed the binning in previous studies, the rotational state is binned to the closest allowed J state, keeping in mind the selection rule for the rotational state of our diatomic molecule: $\Delta J = \pm 2$. With the weighted binning method, the integer rotational state closest to J_f is chosen, and given a weight of $W_i = 2$ when it is allowed, or $W_i = 0$ when it is not allowed, with i for the ith trajectory performed, effectively ignoring any trajectory with a disallowed transition[38]. Assuming an equal distribution over all possible classical rotational energies, this would yield an average total weight equal to the number of trajectories performed. Finally,

with the floor binning method the classical rotational state J_f is rounded
downward towards the first allowed J state, keeping in mind the selection rule.
For both the standard and floor binning, $W_i = 1$ is always chosen for every
trajectory.

With the rotational state (J) determined, the vibrational state (v) is chosen
by finding the rovibrational state that is closest in total rovibrational energy to
the states allowed by the binned rotational state. Trajectories are considered
rovibrationally elastically scattered when the final rovibrational state of H_2 is
binned to the same state as its initial state, and rovibrationally inelastically
scattered when the binned final state is not the same as the initial rovibrational
state. The m_J state is not taken into account at all for the final state, as it is
degenerate with the other possible m_J states.

Reaction and (state-to-state) scattering probabilities are then determined
by dividing the weight of each by the weight of all trajectories. For the standard
and floor binning methods, these probabilities are equal to dividing the number
of reacted or scattered trajectories by the total number of trajectories performed.

5.2.3   Comparisons to experiment

We will also compare our theoretical dissociation curves to those reported in
several experimental studies[7, 8, 11]. The experimental results we discuss are
all obtained from direct inversion of time of flight (ToF) results obtained from
desorption experiments. These inverted data are then fitted to a functional
form, which range from very simplistic to quite advanced. Here we will only
concern ourselves with the very simple error function

$$S(v, J, T_s, E_{kin}) = \frac{A(v, J)}{2}\Big[1 + \mathrm{erf}\Big(\frac{E_{kin} - E_0(v, J)}{W(v, J)}\Big)\Big] \qquad (5.3)$$

where the three fitted variables A, E_0, and W are the saturation value, inflection
point and width respectively. While absolute E_0 and W parameters can be
directly obtained from these inverted ToF spectra, the same cannot be said for
the saturation value, for which only relative values can be found directly. Thus
experimental studies often fit their curves under the assumption of a saturation
value of $A = 1$, while both experimental and theoretical adsorption studies
rarely ever find such a value. Furthermore, care should be taken when scaling
the curves to different saturation values, as some previous studies have found
these three parameters to be not entirely independent[20]. Both references [7]
and [11] have also used beam adsorption experiments to determine absolute
saturation values for their surfaces. It is, however, unclear if these can be

directly applied to their experimental desorption data, due to differences in experimental setup, including surface temperature.

Finally, Kaufmann *et al.* also identified a slow reaction channel, which was fit separately using

$$S_{slow}(v, J, E_{kin}) = A_{slow}(v, J) \exp\left(\frac{-E_{kin}}{\gamma(v, J)}\right) \tag{5.4}$$

where A_{slow} defines the amplitude, and γ a decay parameter[11]. The older works by Rettner *et al.*[7] and Hodgson *et al.*[8] we compare to, as well as all theoretical works to date, did not find this separate channel.

5.3   Results and discussion

5.3.1   Rovibrationally excited states and a dynamic surface

First we will compare the reaction probability curves obtained for both the EAM-SCM and EAM-DCM at a QC level to those obtained using QD-EAM-SCM. Chapter 4 has already shown that the QD- and QCD-EAM-SCM results show excellent agreement for the rovibrational ground state of H_2. However, this has not yet been verified for the rovibrationally excited states or when also considering the moving surface of the EAM-DCM, as previous comparisons between QCD-EAM-SCM and -DCM were only performed for the D_2 scattering reaction[15]. In Figure 5.1, we show some of the reaction probabilities previously obtained for the rovibrational ground state (a), as well as a rotationally excited initial state [(c); v, J = 0, 2]. Similarly for panels (b) and (d) we show the results obtained for the vibrationally excited (v = 1) state, with J = 0 and J = 2, respectively. Next to the QCD- and QD-EAM-SCM results, we also included the QCD- and QD-BOSS results, as well as the QCD-EAM-DCM results.

As expected, the agreement between QCD and QD, both for the BOSS and EAM-SCM results, is very good, with some minor differences in curve width more prominently visible for the vibrationally excited states. The small fluctuations in the SRP48 CRP PES are much more clearly visible for the QD-BOSS results, compared to the QD-EAM-SCM. This is primarily attributed to the averaging over many surfaces we perform to obtain accurate surface temperature effects, as this will smooth out these smaller inconsistencies in the results. The agreement between the QCD-EAM-SCM and -DCM (and thus also with the QD-EAM-SCM) results is again excellent, as was already shown for the D_2/Cu(111) system. This observation is perhaps not too surprising, as the mass mismatch between H_2 and the Cu surface is even bigger than that of

5
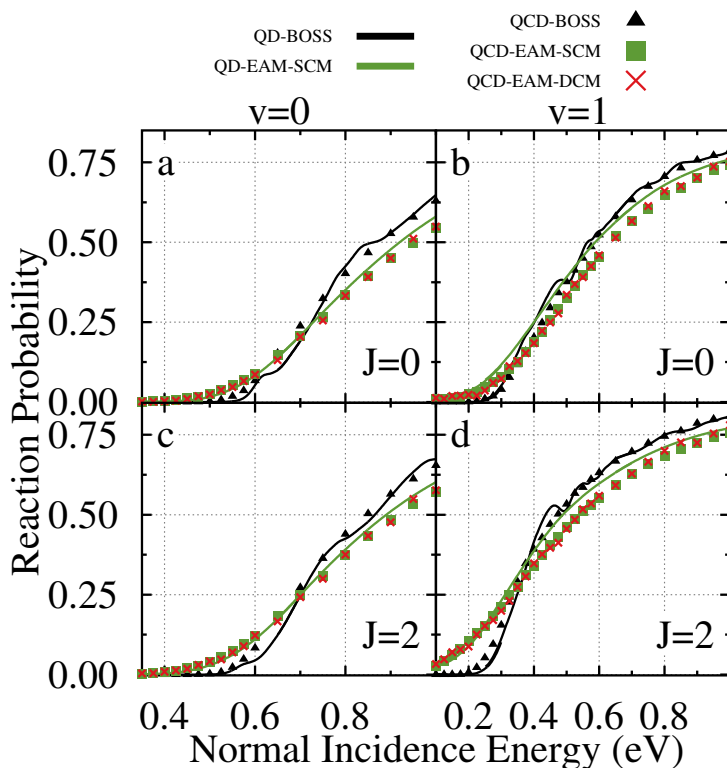

FIGURE 5.1: Reaction probabilities obtained for four initial rovibrational states of H_2 on Cu(111): (a) v = 0, J = 0; (b) v = 1, J = 0; (c) v = 0, J = 2; (d) v = 1, J = 2. Included are the QD- and QCD-EAM-SCM results as a green curve and green squares respectively, QCD-EAM-DCM results as red crosses, and QD- and QCD-BOSS results as a black curve and black triangles respectively. A modeled surface temperature of 925 K was used for the SCM and DCM.

D_2 and Cu, but it once again confirms the validity of the sudden approximation for this system, and demonstrates the (lack of) effect of energy exchange for the dissociation reaction.

5.3.2 Binning methods explored

To achieve the best agreement between QCD and QD results, we also compare three (relatively simple) binning methods to obtain the final rovibrational state of our QCD simulations. This is especially valuable not just for this work, but also for future studies. Finding which QCD binning method compares best compared to rigorous QD simulations will be very important when comparing rovibrationally (in)elastic scattering probabilities. We show the effects of these binning methods on the final dissociation probabilities we compute in Figure 5.2., again for panels (a) the rovibrational ground state, (b) a vibrationally excited state, (c) a rotationally excited state, (d) and a rovibrationally excited state. As only the weighted binning will have an effect on the final reaction probabilities compared to the standard and floor binning, we have not included the floor binning in this figure. We include binned QCD results obtained with both the BOSS and EAM-SCM PES, as well as QD results from those PESs as a comparison.

We find the same trend for all four rovibrational states, with the standard binning method resulting in slightly higher reaction probabilities compared to the weighted binning. This effect is most noticeable for the $J = 0$ states, where the reaction is up to 3 percentpoint higher when using the standard binning method, which could be explained by the lack of lower energy rovibrational states to scatter into compared to the $J = 2$ states. In general, these slightly higher probabilities found using standard binning improves agreement with the QD results, both for BOSS and for EAM-SCM, although this effect is small enough that it will not significantly affect any conclusions made using either method.

The same cannot really be said when considering the rovibrationally elastic scattering curves for the three binning methods we have included. Figure 5.3 and 5.4 present these scattering probabilities for the vibrational ground and first excited state respectively, split for the standard [(a), (d), and (g)], weighted [(b), (e), and (h)], and floor [(c), (f), and (j)] binning methods. Again we take into account the rotational ground state [(a)-(c)]; $J = 0$, but now two additional excited states: [(d)-(f)] $J = 1$, and [(g)-(j)] $J = 2$. Next to the binned QCD-EAM-SCM and QCD-BOSS results, we also included the binned QCD-EAM-DCM results. QD-BOSS and -EAM-SCM results are again included as a comparison.
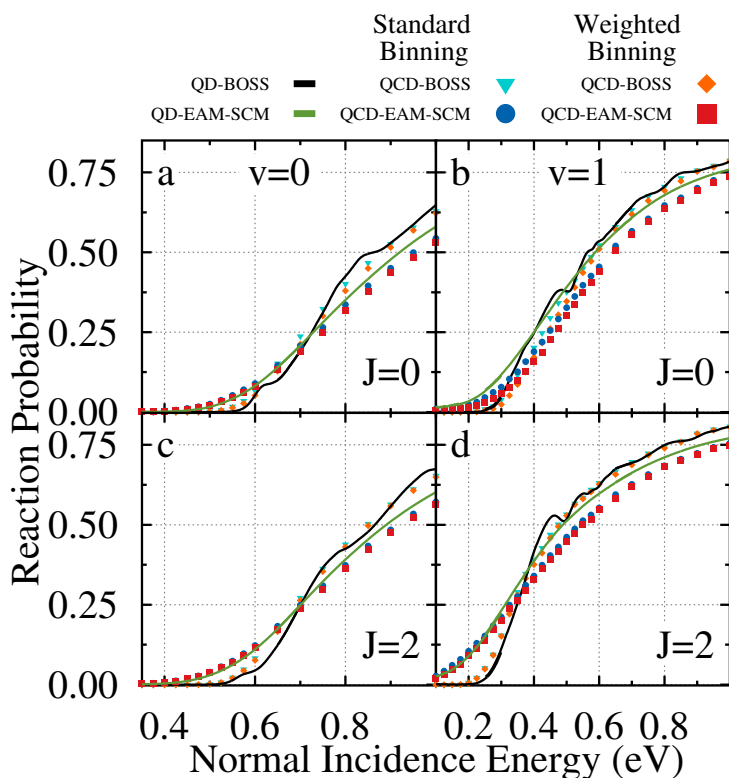
FIGURE 5.2: Reaction probabilities obtained for four initial rovibrational states of H_2 on Cu(111): (a) $v = 0$, $J = 0$; (b) $v = 1$, $J = 0$; (c) $v = 0$, $J = 2$; (d) $v = 1$, $J = 2$. The QD results for the BOSS and EAM-SCM results are shown as black and green curves respectively, while the QCD-BOSS results are displayed as cyan triangles for the standard binning and orange diamonds for weighted binning. The QCD-EAM-SCM results show as blue circles for standard binning, and red squares for weighted binning.

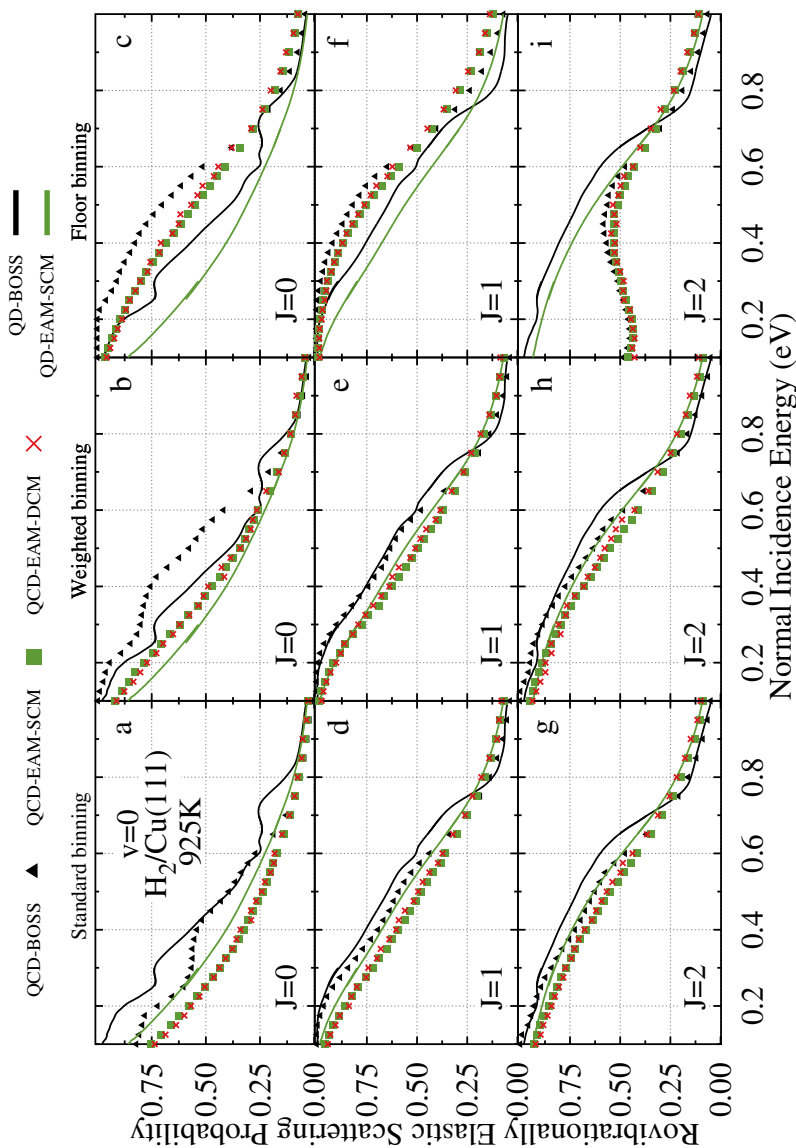A modeled surface temperature of 925 K was used for the SCM and DCM.

FIGURE 5.3: Rovibrationally elastic scattering probabilities of H_2 on a Cu(111) surface, obtained for the vibrational ground state ($v = 0$), and three rotational states: [(a)-(c)] $J = 0$; [(d)-(f)] $J = 1$; and [(g)-(i)] $J = 2$. Results are shown for the [(a), (d), and (g)] standard, [(b), (e), and (h)] weighted, and [(c), (f), and (i)] floor binning methods. Included are QD- and QCD- EAM-SCM results as a green curve and green squares respectively, QD- and QCD-BOSS results as a black curve and black triangles respectively, and finally the QCD-EAM-DCM results as red crosses. A modeled surface temperature of 925 K was used for the SCM and DCM.
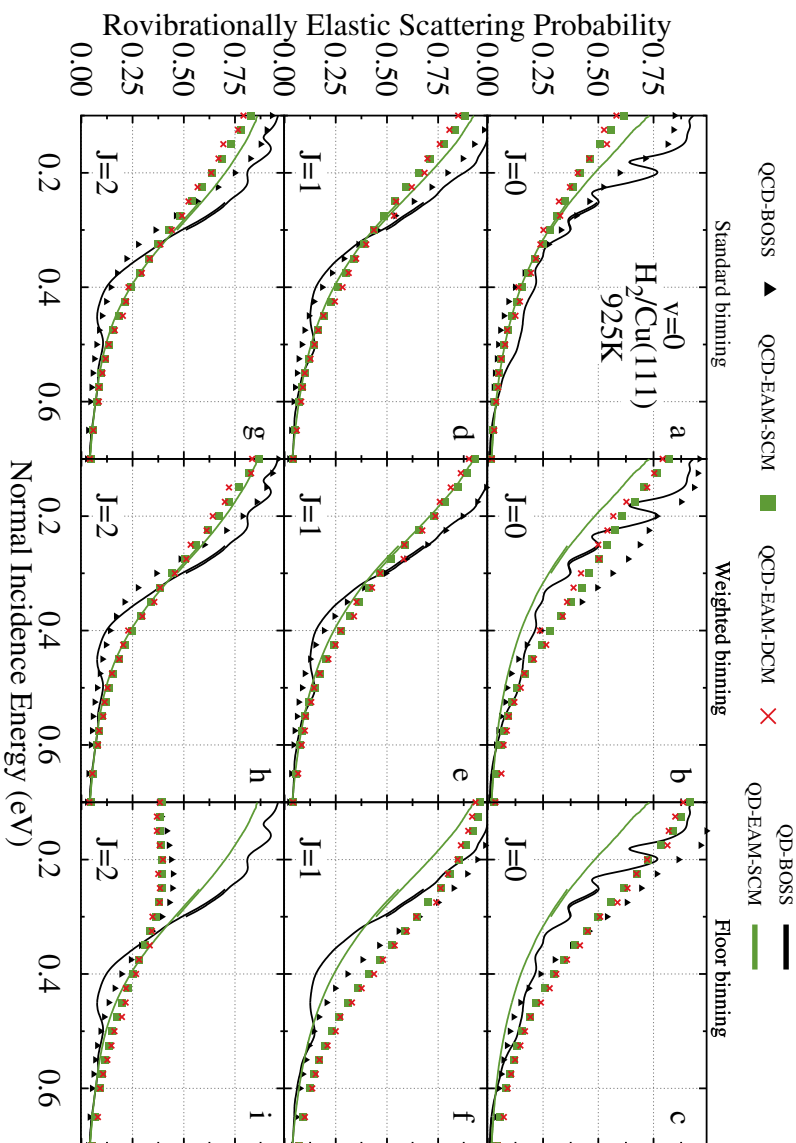
FIGURE 5.4: Rovibrationally elastic scattering probabilities of H_2 on a Cu(111) surface, obtained for the first vibrationally excited state ($v = 1$), and three rotational states: [(a)-(c)] $J = 0$; [(d)-(f)] $J = 1$; and [(g)-(i)] $J = 2$. Results are shown for the [(a), (d), and (g)] standard, [(b), (e), and (h)] weighted, and [(c), (f), and (i)] floor binning methods. Included are QD- and QCD-EAM-SCM results as a green curve and green squares respectively, QD- and QCD-BOSS results as a black curve and black triangles respectively, and finally the QCD-EAM-DCM results as red crosses. A modeled surface temperature of 925 K was used for the SCM and DCM.

As noted before, the agreement between the QCD-EAM-DCM and QCD-EAM-SCM results is again excellent regardless of the binning method chosen. This matches the findings of earlier work for D_2 on Cu(111), and further shows its independence of the binning method used.

The floor binning method heavily overestimates the elastic scattering probabilities at lower incidence energies compared to the QD results, or underestimates when the initial state is not the lowest allowed rotational state available. Interestingly, this also applies for the vibrationally excited states, suggesting that there is little conversion of vibrational to rotational energy, at least at the QCD level. At high incidence energies the agreement with the QD results does appear to be relatively good, although we do not think this binning method is in general a good choice for comparisons to QD results.

We find that the standard binning method generally predicts lower scattering probabilities compared to the weighted binning, which can be partially explained by the slightly higher reaction probabilities found for standard binning. Furthermore, those trajectories that are found with a "classical rotational state" slightly above the first rotational state of the incoming molecule ($\Delta J = +1$) are often binned "upward" to the first allowed state when using standard binning, while these states are completely disregarded for weighted binning. This effect would results in higher probabilities for the lower rotational states when dealing with lower incidence energies, as their energy would not be high enough to "push" the scattered molecules all the way to the next allowed state. We expect this effect to be especially strong for those states where the lowest allowed rotational state is also the initial state, in our results $J = 0$ and $J = 1$, and to be much more important for the scattering results, compared to the dissociation probabilities. However, it appears to be clearly noticeable only for the rovibrational ground state, where there is no vibrational energy to convert to higher rotational states, and to be somewhat important for the $v = 1$, $J = 0$ state. Neither of the $J = 1$ states show any significant difference that we can ascribe to this binning effect.

In general, the QCD binning method that leads to the best agreement with the QD results appears to heavily depend on the initial rovibrational state of the H_2. The standard binning performs somewhat better than the weighted binning for the $v = 0$ states and the $v = 1$, $J = 0$ state, while the weighted binning method performs a bit better for the $v = 1$, $J = 1, 2$ states, although not by much. The standard binning method underestimates the elastic scattering probabilities for the $v = 1$ states primarily at the lower incidence energies, where reaction is also lower. The weighted binning instead overestimates the $v=1$, $J=0$ probabilities much more over the entire energy range, but shows almost perfect agreement for the rotationally excited states.

For further comparisons to experimental work, the QCD results we present will be obtained using the standard binning method, as it is the method used in our previous studies. However, future work could focus on applying more complicated Gaussian binning methods, which have shown to improve agreement with QD results when properly used[38, 39].

5.3.3 Comparisons to experiment

Having chosen a binning method that yields QCD results that accurately reproduce our QD curves, we next aim to further validate the (QD-)EAM-SCM approach by comparing our reaction probability curves to those obtained in experimental studies. The three studies we compare to - published by Rettner *et al.*[7], Hodgson *et al.*[8] and Kaufmann *et al.*[11] - all obtained their results from desorption experiments, from direct inversion of their ToF results under the assumption of detailed balance.

As we discuss in section 5.2.3, this allows these studies to fit absolute values of the width parameter (W) and the inflection point (E_0) as described in equation 5.3. However, only relative saturation values (A) can be obtained from these experiments. Several approaches were suggested to obtain saturation values that allow for an accurate comparison to our theoretical results.

First, both Rettner *et al.* and Kaufmann *et al.* have performed beam adsorption experiments on their surfaces, which would yield accurate absolute saturation values of $A^{Rett} = 0.25$ eV and $A^{Kauf} = 0.35$ eV respectively. However, due to differences in experimental conditions it is unclear if this can directly apply[11]. Primarily the much lower surface temperature of 120 K (vs 925 K here), the use of an incidence angle to vary the normal incidence energy of the molecular beam and the final rovibrational composition of this beam could all have an effect on the final results of the adsorption measurements when compared to the desorption experiments. Additional discussion on these differences can be found in Ref. [11]. Next, it is suggested to use the theoretical curves to estimate an appropriate saturation value, by setting the saturation value to be equal to the theoretical sticking probability at the incidence energy to which the experiment is sensitive[11]. This will generally yield values in the range 0.50–0.60 eV. Finally, Wijzenbroek and Somers also found very good agreement between the experimental results of Hodgson *et al.* and Rettner *et al.* when the saturation for the Hodgson results is chosen as two times that of the Rettner curve $(A^{Hodg} = 0.50$ eV)[20].

In Figure 5.5 we present these fitted experimental S-curves and compare them to our QD- and QCD-EAM-SCM results. We have again included the initial rovibrational states of $(v, J) = (0, 0), (0, 1), (0, 2), (1, 0), (1, 1)$, and $(1, 2)$
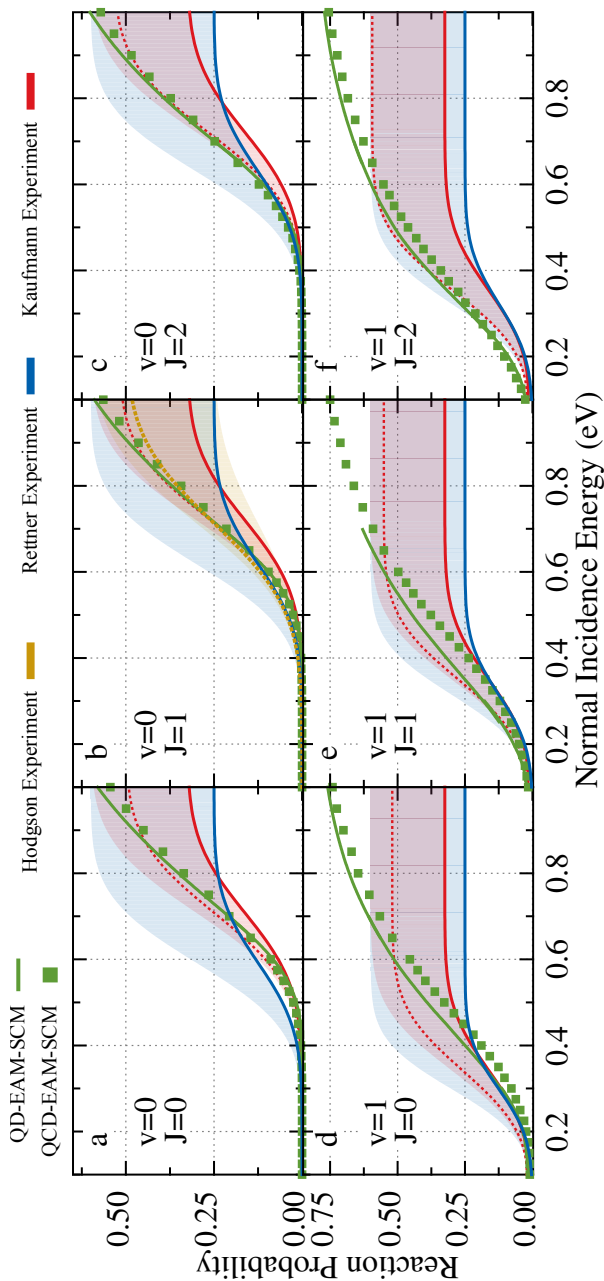
FIGURE 5.5: Reaction probabilities obtained for six initial rovibrational states of H_2 on Cu(111): (a) $v = 0$, $J = 0$; (b) $v = 0$, $J = 1$; (c) $v = 0$, $J = 2$; (d) $v = 1$, $J = 0$; (e) $v = 1$, $J = 1$; (f) $v = 1$, $J = 2$. Theoretical QD- and QCD-EAM-SCM results are shown as a green curve and green squares respectively. The experimental curves by Hodgson et al.[8], Rettner et al.[7] and Kaufmann et al.[11] are included in orange, blue and red respectively, with the uncertainty in the saturation value parameters of the experimental fits shown as shaded areas. Specific experimental curves are highlighted as: (solid red / solid blue) $A_0 = 0.5$ and 0.25 eV respectively from adsorption experiments; (dashed red) saturation parameter set equal to experimental QCD-EAM-SCM value at 0.95 eV; (dashed orange) estimated $A_0 = 0.25$ value based on agreement with Rettner experiment. A (modeled) surface temperature of 925 K was used for all these results.

for (a)-(f), respectively. The uncertainty in the saturation values are shown as shaded areas for each of the curves, choosing as a minimum the results from the beam adsorption experiments when available, or $A_{Min}^{Hodg} = 0.25$ for the curve where these data are not available. As a maximum a value of $A = 0.60$ eV is chosen, as no experimental works to our knowledge have reported values higher than this. Thus the shaded areas of each color reflect the range of A parameters [see (5.3)] each of the experimental curves could have, and visualises the uncertainty in the experimental absolute saturation values. Also included as solid lines are those curves where experimental beam adsorption results were used to obtain saturation values, when available for the experimental study, however these did not use exactly the same conditions as the desorption experiments that were fitted originally.

Finally, the estimated saturation values for the work by Hodgson *et al.*, based on the experimental work by Rettner *et al.*, and those estimated based on the theoretical sticking probabilities are included as dashed lines in orange and red respectively. The theoretically estimated saturation values of the Kaufmann experimental fit are set to be equal to our QCD-EAM-SCM results at the highest available energy of the experimental results, as has been done in previous studies[11, 21].

Comparing the experimental results to each other, keeping in mind especially the uncertainty in saturation values, we find good agreement. Only for the rovibrational ground state do we find some disagreement for the curve onset, which cannot be directly explained by this uncertainty. Interestingly, the experimentally obtained curves with saturation values predicted based on the desorption experiments (shown as solid lines in blue and red) show much better agreement for the vibrationally excited states compared to the vibrational ground state. Kaufmann *et al.* make a similar observation when directly comparing experimentally obtained E_0 and W parameters. They believe this disagreement to be primarily caused by errors in the calibration of the older works by Rettner *et al.*, which primarily affected accurate analysis of the faster (less rovibrationally excited) molecules[11].

We had already previously noted the generally good agreement between the QCD- and QCD-EAM-SCM results for some of these rovibrational states, although the differences for the vibrationally excited states is also clearly present for the v = 0, J = 1 state, with the QD results predicting a slightly higher dissociation probability across the entire energy range investigated.

Choosing the experimental saturation values based on the theoretical sticking values, in particular, leads to great agreement, as can be seen when comparing the red dashed line to our theoretical results in green for every state except v = 1, J = 0. For this state in particular we do see excellent overlap between

the QD-EAM-SCM results and the results presented by Kaufmann *et al.*, with a saturation value based on their beam adsorption experiments. Overall agreement between the theoretical work and the experimental work is good, with the theoretical results falling well within the range of experimental saturation values we expect.

5.3.4 Logscale results

To more carefully inspect the curve onset of our dissociation results, we have plotted them again on a logarithmic scale. In Figure 5.6. we again present our QD- and QCD-EAM-SCM, QD- and QCD-BOSS results, as well as the QCD-EAM-DCM results, where a moving surface is included. The rovibrational states are the same as presented in Figure 5.1., also using the same curves and symbols.

One of the first things that can be clearly noticed is the unexpected noise, or unexpected curvature, found in the QD results of both the BOSS and EAM-SCM results. As the reaction probabilities reach very low values, noise from our QD implementation starts becoming a much more important factor of the final results. This noise can clearly be seen in the unphysical behaviour in the BOSS curves, when considering the vibrational ground state (a) and (c) results at low incidence energies. One of the main contributions of this noise, we believe, is the error inherent to the SPO method in Eq. 6.1, which is inherent to the step-wise integration method of the SPO and scales with Δt^3. Thus smaller and smaller time steps are needed to accurately describe reaction probabilities ($P \approx 10^{-3}$), much lower than those we have used for our calculations (see 6.A). Reducing the time step by a factor 10 should reduce the expected noise due to the SPO propagation by as much as a factor of 10^3 while only increasing the computational load by a factor of 10. However, other factors and parameters of the WPs would also start to play a more dominant role in the final error that we observe. We consider the additional computational time needed to properly sample enough distorted surfaces for the SCM while also reducing this time step to be unfeasible for this study, although we believe it could be an important topic for later work.

Those results that we expect to be either partially, or perhaps fully, dominated by this noise we have included using a different curve color, with a lighter shade of either black for BOSS or green for the EAM-SCM results. However, an upturn of the reaction probability does seem to appear for very low incidence energies which is not visible at all for our QCD results. Recent work by Dutta *et al.* report a similar upturn for the $D_2/Cu(111)$ system, investigated with the same SRP48 BOSS PES and QD implementation, but using the effective
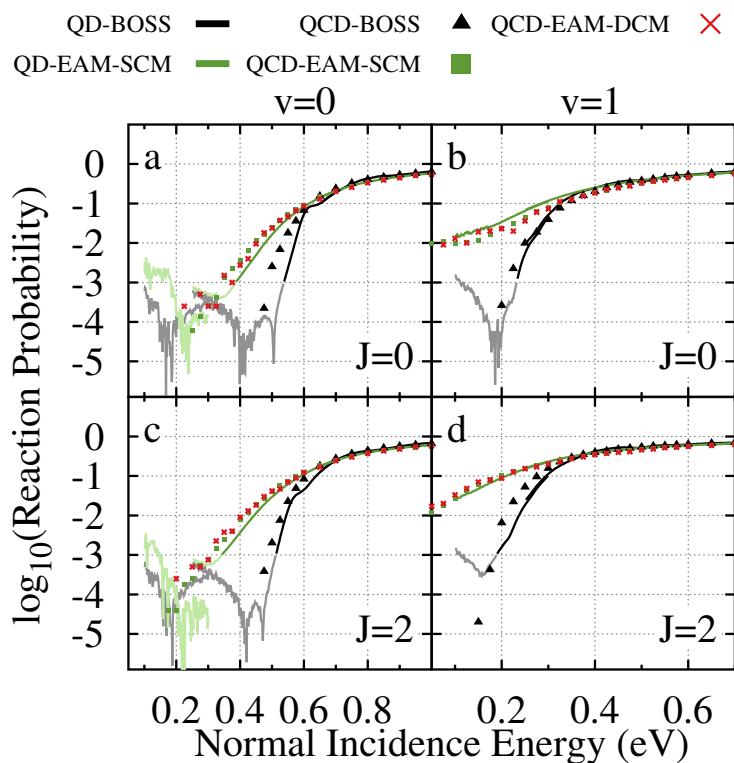
FIGURE 5.6: Reaction probabilities obtained for four initial rovibrational states of H_2 on Cu(111): (a) v = 0, J = 0; (b) v = 1, J = 0; (c) v = 0, J = 2; (d) v = 1, J = 2, with the reaction probabilities on a logarithmic scale. Theoretical QD- and QCD-EAM-SCM results are shown as a green curve and green squares respectively, and QD- and QCD-BOSS results as a black curve and black triangles, respectively. QD results where noise is expected to play a major role are shown as a lighter shade curve. QCD-EAM-DCM results are included as red crosses. A modeled surface temperature of 925 K was used for all the SCM and DCM results.

Hartree potential method, to include surface temperature effects[40]. They believe this could be attributed to the vibrational degrees of freedom, due to a modeled elevated surface temperature, which could match the slow channel as reported by Kaufmann *et al.*[11]. This EfHP work, however, uses the same SPO propagation method and is thus also expected to exhibit errors of a similar magnitude as our work, which is covered in both works. Furthermore, we also observe an upturn for the ideal lattice BOSS model, which suggests something more than purely attributing this to surface vibrational DoF. Thus, this would be a prime target for further studies, using more carefully crafted WPs and employing much smaller time steps in the SPO to investigate the very low incidence energy regions of our H_2 on the Cu(111) system, because at the moment we also do not yet have theoretical explanations of why such an upturn should be present in our BOSS results.

For the higher incidence energies, where the error in our QD results is expected to be small, we do still see great agreement with the QCD results, both for the BOSS and EAM-SCM results. The much more rapid drop in reactivity as the incidence energy decreases seen in the BOSS results, when compared to the EAM-SCM results, matches the observation of increased curve broadness when higher surface temperatures are taken into account[20, 21, 41]. For both PESs and every initial rovibrational state, the QCD calculations yield slightly higher reaction probabilities, except for the EAM-SCM results of the $v = 1$, $J = 0$ state, where this relation is inverted. This confirms again the quality of the EAM-SCM implementation at a QD level, and shows that we can accurately include the thermal surface effects into our QD simulations, even at lower energies. Furthermore, the EAM-DCM results almost perfectly match those of the EAM-SCM. This again shows the validity of a static surface approximation for our specific system, and the minimal effect energy exchange has for this dissociation reaction.

Finally, in Figure 5.7 we will compare the curve onset of our theoretical dissociation curves to those found in the experimental studies that we considered. The same states and results are presented as we had shown in Figure 5.5., but now we also included the QD- and QCD-BOSS results. Again we have used shaded areas to mark the uncertainty in the absolute experimental *A* values, which appears as a small static shift on the logarithmic scale. Furthermore, the contribution of the slow reaction channel reported by Kaufmann *et al.* now also becomes much more apparent at low incidence energies. Neither the work by Rettner *et al.* nor the work by Hodgson *et al.* reported observing this channel in their work.

Overlap between our QD- and QCD-EAM-SCM curves and the experimental results of Kaufmann *et al.* is, in general, excellent even for very low reaction
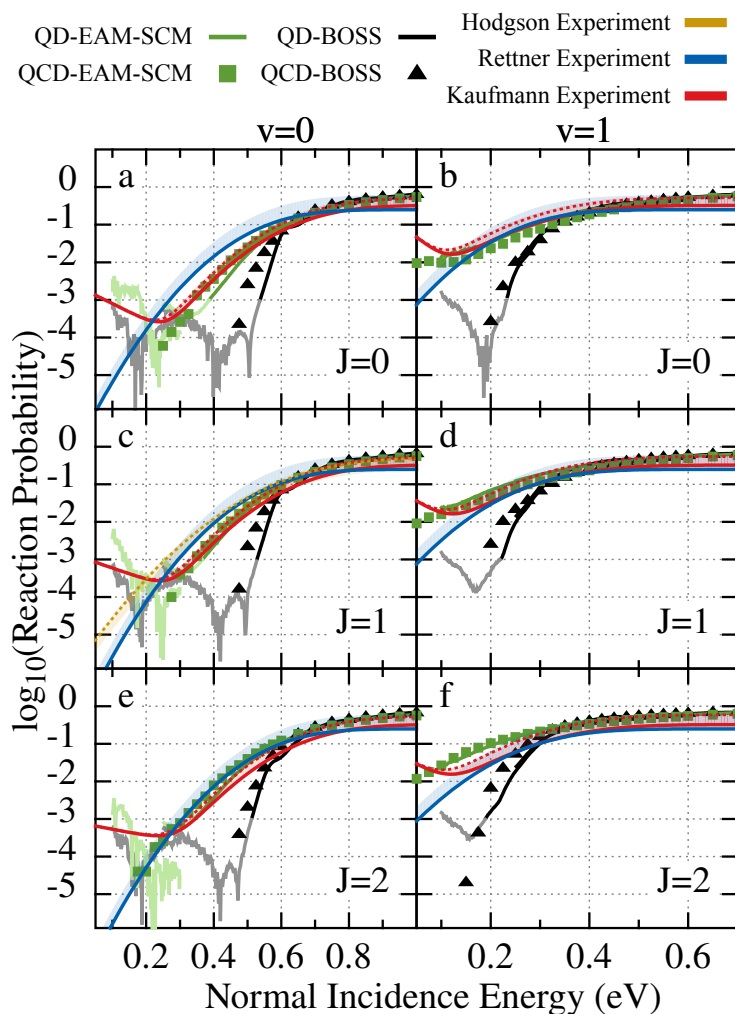
FIGURE 5.7:   Reaction probabilities obtained for six initial rovibrational states of H$_2$ on Cu(111): (a) v = 0, J = 0; (b) v = 1, J = 0; (c) v = 0, J = 1; (d) v = 1, J = 1; (e) v = 0, J = 2; (f) v = 1, J = 2, with the reaction probabilities on a logarithmic scale. Theoretical QD- and QCD-EAM-SCM results are shown as a green curve and green squares respectively, and QD- and QCD-BOSS results as a black curve and black triangles, respectively. QD results where noise is expected to play a major role are shown as a lighter shade. The experimental curves by Hodgson *et al.*[8], Rettner *et al.*[7] and Kaufmann *et al.*[11] are included in orange, blue and red respectively, with the uncertainty in the saturation value parameters of the experimental fits shown as shaded areas. Additional curves are shown the same as in Figure 5.5. A (modeled) surface temperature of 925 K was used for all these results.

probabilities. The biggest differences are found for the rovibrational ground state and the highest excited state that we included (v = 1, J = 2). However, a clear difference is found for the QCD-EAM-SCM results at very low incidence energies, as they do not predict any kind of slow channel. While the QD-EAM-SCM, and even the QD-BOSS, results do appear to predict an increase in reactivity at these very low energies, it is at the moment still unclear if this is an actual physical effect or an artifact introduced by our QD approach (or the CRP BOSS PES). Nevertheless, an upturn has been observed both in this study, and by Dutta *et al.* using a similar QD approach, but with a different method for including surface temperature effects, but also using the same BOSS PES and the same V_{coup} of the SCM to construct the effective time-dependent Hartree potential[40]. Again it should be emphasised that this work, as well as the work of Dutta *et al.*, is still as of yet inconclusive given the expected magnitude of errors in the QD simulations for these low probabilities. Fascinating though is the suggested presence of the apparent signal, even in our older BOSS calculations, and as of yet we lack an explanation for it (predominantly because of the errors in the approximations that we have to make in the QD). Thus, a more thorough theoretical investigation of this upturn, both with the SCM and the EfHP method, would be a very important topic for further studies. However, these computations will be computationally challenging, as reducing the time step by a factor of 10 will increase the computational costs by a factor of 10. Especially when also considering this for T_s = 925 K. One then has to perform these ten times more expensive calculations for at least 100 individual surface configurations, making such a study truly state-of-the-art and currently out of the scope for this paper.

5.4 Conclusion

We investigated the quality of the EAM-SCM approach, including all relevant surface temperature effects, at both a quantum dynamical and quasi-classical level, using the dissociative chemisorption of H_2 on Cu(111) (at a surface temperature of 925 K) as a model system. We computed both reaction and rovibrationally elastic scattering probabilities, and compared those to values obtained from the dynamic surface EAM-DCM and to H_2 sticking curves from experimental studies. We also investigated several simple binning methods, to validate the agreement between the QCD probabilities, and those obtained using rigorous quantum dynamics simulations. Our BOSS PES was constructed by Nattino *et al.*[29] using the CRP, with datapoints obtained from DFT using the SRP48 functional, while the SCM distorted surface corrections were described by the effective three-body SCM coupling potential as published by Spiering

et al.[25]. The thermally distorted surface configurations for the SCM were obtained from a highly accurate EAM potential using molecular dynamics, as described in Chapter 3.

While previous work had already shown that the QCD- and QD-EAM-SCM dissociation probabilities agreed well for the rovibrational ground state, we that demonstrated this also holds true for several initially rovibrationally excited states. The three different binnings methods that we investigated did not appear to significantly affect these probabilities, although weighted binning did slightly reduce the predicted QCD reaction probabilities, which reduced agreement with the QD curves.

Larger effects were found for the rovibrational elastic scattering, where either this weighted binning or our standard binning demonstrated better agreement with the curves obtained from QD simulations, for both the EAM-SCM and the BOSS approach. The final method of binning - floor binning - was found to greatly overestimate rovibrationally elastic scattering probabilities for the lower energy rovibrational states, but then greatly underestimated the same probabilities for those states that had more rovibrational energy available and had allowed scattering states with similar energies. As it only affected the determination of the final state of scattered molecules, the floor binning did not change the reaction probabilities compared to our standard binning method. Overall, we believe both the standard and weighted binning methods performed equally well, and as such could both be of interest for further studies.

Taking into account the uncertainty in absolute experimental saturation values, due to the nature of the direct inversion of desorption results used in the experimental method, we also found excellent agreement between our (QD-)EAM-SCM results and the experimental curves published by Rettner *et al.*[7], Hodgson *et al.*[8] and Kaufmann *et al.*[11]. Even for the curve onset, where reaction is best plotted on a logarithmic scale, we see good overlap with our theoretical results. At very low incidence energies, our QD results even indicate a small upturn in reaction similar to those found by Kaufmann *et al.*, also found by Dutta *et al.* using their EfHP method and the same QD code[40], but not been reported before in any other theoretical works. However, great care should be taken when interpreting our QD results in this regime, as the very low probabilities involved enables the noise inherent to the SPO method to become an important contribution to our final results. More carefully constructed wave packets, using a much smaller time step to minimise the error when propagating, would allow for a more thorough analysis of this slow channel using QD simulations.

In general, this work has shown that the EAM-SCM approach, which included surface temperature effects into quasi-classical and quantum dynamical

simulations works well for the H_2 on the Cu(111) system, at least at a surface temperature of 925 K. Comparisons to the dynamic surface EAM-DCM results further validate the sudden approximation made in the model, while comparisons to experimental results show that the model holds both for the rovibrational ground state, as well as several rovibrationally excited states. However, several other observables found in the literature, such as rotational/vibrational efficacies and rovibrationally inelastic scattering probabilities, have not yet been verified and thus are an interesting subject for further study. Equally, the noise introduced by the SPO method made it difficult to convincingly show that the slow channel of the H_2/Cu(111) system can be observed at a theoretical level using the EAM-SCM and thus would be an excellent target for further work, both using our SCM and the EfHP method by Dutta *et al.*

5

References

(1)   Chorkendorff, I., *Concepts of Modern Catalysis and Kinetics*; Wiley-VCH: Weinheim, 2003.

(2)   Smith, C.; Hill, A. K.; Torrente-Murciano, L. Current and future role of Haber–Bosch ammonia in a carbon-free energy landscape. *Energy & Environmental Science* **2020**, *13*, 331–344, DOI: 10.1039/C9EE02873K.

(3)   Campbell, C. T. The Degree of Rate Control: A Powerful Tool for Catalysis Research. *ACS Catalysis* **2017**, *7*, 2770–2779, DOI: 10.1021/acscatal.7b00115.

(4)   Kroes, G.-J. Computational approaches to dissociative chemisorption on metals: towards chemical accuracy. *Physical Chemistry Chemical Physics* **2021**, *23*, 8962–9048, DOI: 10.1039/D1CP00044F.

(5)   Berger, H. F.; Leisch, M.; Winkler, A.; Rendulic, K. D. A Search for Vibrational Contributions to the Activated Adsorption of H$_2$ on Copper. *Chemical Physics Letters* **1990**, *175*, 425–428, DOI: 10.1016/0009-2614(90)85558-T.

(6)   Michelsen, H. A.; Rettner, C. T.; Auerbach, D. J.; Zare, R. N. Effect of rotation on the translational and vibrational energy dependence of the dissociative adsorption of D$_2$ on Cu(111). *The Journal of Chemical Physics* **1993**, *98*, 8294–8307, DOI: 10.1063/1.464535.

(7)   Rettner, C. T.; Michelsen, H. A.; Auerbach, D. J. Quantum-state-specific dynamics of the dissociative adsorption and associative desorption of H$_2$ at a Cu(111) surface. *The Journal of Chemical Physics* **1995**, *102*, 4625–4641, DOI: 10.1063/1.469511.

(8)   Hodgson, A.; Samson, P.; Wight, A.; Cottrell, C. Rotational Excitation and Vibrational Relaxation of H$_2$ Scattered from Cu(111). *Physical Review Letters* **1997**, *78*, 963–966, DOI: 10.1103/PhysRevLett.78.963.

(9)   Hou, H.; Gulding, S. J.; Rettner, C. T.; Wodtke, A. M.; Auerbach, D. J. The Stereodynamics of a Gas-Surface Reaction. *Science* **1997**, *277*, 80–82, DOI: 10.1126/science.277.5322.80.

(10)   Murphy, M. J.; Hodgson, A. Adsorption and desorption dynamics of H$_2$ and D$_2$ on Cu(111): The role of surface temperature and evidence for corrugation of the dissociation barrier. *The Journal of Chemical Physics* **1998**, *108*, 4199–4211, DOI: 10.1063/1.475818.

(11)   Kaufmann, S.; Shuai, Q.; Auerbach, D. J.; Schwarzer, D.; Wodtke, A. M. Associative desorption of hydrogen isotopologues from copper surfaces: Characterization of two reaction mechanisms. *The Journal of Chemical Physics* **2018**, *148*, 194703, DOI: 10.1063/1.5025666.

(12)   Chadwick, H.; Somers, M. F.; Stewart, A. C.; Alkoby, Y.; Carter, T. J. D.; Butkovicova, D.; Alexandrowicz, G. Stopping Molecular Rotation Using Coherent Ultra-Low-Energy Magnetic Manipulations. *Nature Communications* **2022**, *13*, 2287, DOI: 10.1038/s41467-022-29830-3.

(13)   Díaz, C.; Pijper, E.; Olsen, R. A.; Busnengo, H. F.; Auerbach, D. J.; Kroes, G. J. Chemically accurate simulation of a prototypical surface reaction: H_2 dissociation on Cu(111). *Science (New York, N.Y.)* **2009**, *326*, 832–834, DOI: 10.1126/science.1178722.

(14)   Galparsoro, O.; Kaufmann, S.; Auerbach, D. J.; Kandratsenka, A.; Wodtke, A. M. First Principles Rates for Surface Chemistry Employing Exact Transition State Theory: Application to Recombinative Desorption of Hydrogen from Cu(111). *Physical Chemistry Chemical Physics* **2020**, *22*, 17532–17539, DOI: 10.1039/D0CP02858D.

(15)   Smits, B.; Somers, M. F. Beyond the static corrugation model: Dynamic surfaces with the embedded atom method. *The Journal of Chemical Physics* **2021**, *154*, 074710, DOI: 10.1063/5.0036611.

(16)   Smeets, E. W. F.; Kroes, G.-J. Designing New SRP Density Functionals Including Non-Local vdW-DF2 Correlation for H_2 + Cu(111) and Their Transferability to H_2 + Ag(111), Au(111) and Pt(111). *Physical Chemistry Chemical Physics* **2021**, *23*, 7875–7901, DOI: 10.1039/D0CP05173J.

(17)   Smeets, E. W. F.; Kroes, G.-J. Performance of Made Simple Meta-GGA Functionals with rVV10 Nonlocal Correlation for H_2 + Cu(111), D_2 + Ag(111), H_2 + Au(111), and D_2 + Pt(111). *The Journal of Physical Chemistry C* **2021**, *125*, 8993–9010, DOI: 10.1021/acs.jpcc.0c11034.

(18)   Smits, B.; Litjens, L. G. B.; Somers, M. F. Accurate Description of the Quantum Dynamical Surface Temperature Effects on the Dissociative Chemisorption of H_2 from Cu(111). *The Journal of Chemical Physics* **2022**, *156*, 214706, DOI: 10.1063/5.0094985.

(19)   Díaz, C.; Olsen, R. A.; Auerbach, D. J.; Kroes, G. J. Six-Dimensional Dynamics Study of Reactive and Non Reactive Scattering of H_2 from Cu(111) Using a Chemically Accurate Potential Energy Surface. *Physical Chemistry Chemical Physics* **2010**, *12*, 6499–6519, DOI: 10.1039/C0019 56A.

5

(20)   Wijzenbroek, M.; Somers, M. F. Static surface temperature effects on the dissociation of H_2 and D_2 on Cu(111). *The Journal of Chemical Physics* **2012**, *137*, 054703, DOI: 10.1063/1.4738956.

(21)   Nattino, F.; Genova, A.; Guijt, M.; Muzas, A. S.; Díaz, C.; Auerbach, D. J.; Kroes, G.-J. Dissociation and recombination of D_2 on Cu(111): ab initio molecular dynamics calculations and improved analysis of desorption experiments. *The Journal of Chemical Physics* **2014**, *141*, 124705, DOI: 10.1063/1.4896058.

(22)   Bonfanti, M.; Somers, M. F.; Díaz, C.; Busnengo, H. F.; Kroes, G.-J. 7D Quantum Dynamics of H_2 Scattering from Cu(111): The Accuracy of the Phonon Sudden Approximation. *Zeitschrift für Physikalische Chemie* **2013**, 130617035227002, DOI: 10.1524/zpch.2013.0405.

(23)   Mondal, A.; Wijzenbroek, M.; Bonfanti, M.; Díaz, C.; Kroes, G.-J. Thermal Lattice Expansion Effect on Reactive Scattering of H_2 from Cu(111) at T_s = 925 K. *The Journal of Physical Chemistry A* **2013**, *117*, 8770–8781, DOI: 10.1021/jp4042183.

(24)   Kroes, G.-J.; Juaristi, J. I.; Alducin, M. Vibrational Excitation of H_2 Scattering from Cu(111): Effects of Surface Temperature and of Allowing Energy Exchange with the Surface. *The Journal of Physical Chemistry C* **2017**, *121*, 13617–13633, DOI: 10.1021/acs.jpcc.7b01096.

(25)   Spiering, P.; Wijzenbroek, M.; Somers, M. F. An improved static corrugation model. *The Journal of Chemical Physics* **2018**, *149*, 234702, DOI: 10.1063/1.5058271.

(26)   Zhu, L.; Zhang, Y.; Zhang, L.; Zhou, X.; Jiang, B. Unified and transferable description of dynamics of H_2 dissociative adsorption on multiple copper surfaces *via* machine learning. *Physical Chemistry Chemical Physics* **2020**, *22*, 13958–13964, DOI: 10.1039/D0CP02291H.

(27)   Chadwick, H.; Alkoby, Y.; Cantin, J. T.; Lindebaum, D.; Godsi, O.; Maniv, T.; Alexandrowicz, G. Molecular spin echoes; multiple magnetic coherences in molecule surface scattering experiments. *Physical Chemistry Chemical Physics* **2021**, *23*, 7673–7681, DOI: 10.1039/D0CP05399F.

(28)   Busnengo, H. F.; Salin, A.; Dong, W. Representation of the 6D potential energy surface for a diatomic molecule near a solid surface. *The Journal of Chemical Physics* **2000**, *112*, 7641–7651, DOI: 10.1063/1.481377.

(29) Nattino, F.; Díaz, C.; Jackson, B.; Kroes, G.-J. Effect of Surface Motion on the Rotational Quadrupole Alignment Parameter of D_2 Reacting on Cu(111). *Physical Review Letters* **2012**, *108*, 236104, DOI: 10.1103/ PhysRevLett.108.236104.

(30) Kroes, G.-J.; Díaz, C. Quantum and classical dynamics of reactive scattering of H_2 from metal surfaces. *Chemical Society Reviews* **2016**, *45*, 3658–3700, DOI: 10.1039/c5cs00336a.

(31) Sheng, H. W.; Kramer, M. J.; Cadien, A.; Fujita, T.; Chen, M. W. Highly optimized embedded-atom-method potentials for fourteen fcc metals. *Physical Review B* **2011**, *83*, 134118, DOI: 10.1103/PhysRevB.83. 134118.

(32) Spiering, P.; Meyer, J. Testing Electronic Friction Models: Vibrational De-excitation in Scattering of H_2 and D_2 from Cu(111). *The Journal of Physical Chemistry Letters* **2018**, *9*, 1803–1808, DOI: 10.1021/acs. jpclett.7b03182.

(33) Sementa, L.; Wijzenbroek, M.; van Kolck, B. J.; Somers, M. F.; Al-Halabi, A.; Busnengo, H. F.; Olsen, R. A.; Kroes, G. J.; Rutkowski, M.; Thewes, C.; Kleimeier, N. F.; Zacharias, H. Reactive scattering of H_2 from Cu(100): Comparison of dynamics calculations based on the specific reaction parameter approach to density functional theory with experiment. *The Journal of Chemical Physics* **2013**, *138*, 044708, DOI: 10.1063/1.4776224.

(34) Smeets, E. W. F.; Füchsel, G.; Kroes, G.-J. Quantum Dynamics of Dissociative Chemisorption of H_2 on the Stepped Cu(211) Surface. *The Journal of Physical Chemistry C* **2019**, *123*, 23049–23063, DOI: 10. 1021/acs.jpcc.9b06539.

(35) Füchsel, G.; Klamroth, T.; Monturet, S.; Saalfrank, P. Dissipative Dynamics within the Electronic Friction Approach: The Femtosecond Laser Desorption of H_2/D_2 from Ru(0001). *Physical Chemistry Chemical Physics* **2011**, *13*, 8659, DOI: 10.1039/c0cp02086a.

(36) Maurer, R. J.; Jiang, B.; Guo, H.; Tully, J. C. Mode Specific Electronic Friction in Dissociative Chemisorption on Metal Surfaces: H_2 on Ag(111). *Physical Review Letters* **2017**, *118*, 256001, DOI: 10.1103/PhysRevLett. 118.256001.

(37) Spiering, P.; Shakouri, K.; Behler, J.; Kroes, G.-J.; Meyer, J. Orbital-Dependent Electronic Friction Significantly Affects the Description of Reactive Scattering of N_2 from Ru(0001). *The Journal of Physical Chemistry Letters* **2019**, *10*, 2957–2962, DOI: 10.1021/acs.jpclett.9b00523.

5

(38)   Rodríguez-Fernández, A.; Bonnet, L.; Crespos, C.; Larrégaray, P.; Díez Muiño, R. When Classical Trajectories Get to Quantum Accuracy: The Scattering of H₂ on Pd(111). *The Journal of Physical Chemistry Letters* **2019**, *10*, 7629–7635, DOI: `10.1021/acs.jpclett.9b02742`.

(39)   Rodríguez-Fernández, A.; Bonnet, L.; Crespos, C.; Larrégaray, P.; Díez Muiño, R. When Classical Trajectories Get to Quantum Accuracy: II. The Scattering of Rotationally Excited H₂ on Pd(111). *Physical Chemistry Chemical Physics* **2020**, *22*, 22805–22814, DOI: `10.1039/D0CP02655G`.

(40)   Dutta, J.; Naskar, K.; Adhikari, S.; Spiering, P.; Meyer, J.; Somers, M. F. Effect of surface temperature on quantum dynamics of D₂ on Cu(111) using a chemically accurate potential energy surface, To Be Submitted, 2022, submitted.

(41)   *Dynamics of Gas-Surface Interactions: Atomic-level Understanding of Scattering Processes at Surfaces*; Muino, R. D., Busnengo, H. F., Eds.; Springer Series in Surface Sciences; Springer-Verlag: Berlin Heidelberg, 2013, DOI: `10.1007/978-3-642-32955-5`.